Bose Condensation at ^{4}He Interfaces

E. W. Draeger

Lawrence Livermore National Laboratory, 7000 East Avenue, L-415, Livermore, CA 94550

D. M. Ceperley

Department of Physics and National Center for Supercomputing Applications,
University of Illinois Urbana-Champaign, IL 61801

Path Integral Monte Carlo was used to calculate the Bose-Einstein condensate fraction at the surface of a helium film at $T = 0.77$ K, as a function of density[1]. Moving from the center of the slab to the surface, the condensate fraction was found to initially increase with decreasing density to a maximum value of 0.9, before decreasing. Long wavelength density correlations were observed in the static structure factor at the surface of the slab. A surface dispersion relation was calculated from imaginary-time density-density correlations.

Similar calculations of the superfluid density throughout ^{4}He droplets doped with linear impurities $(HCN)_n$ are presented[2]. After deriving a local estimator for the superfluid density distribution, we find a decreased superfluid response in the first solvation layer. This effective normal fluid exhibits temperature dependence similar to that of a two-dimensional helium system.

I. BOSE CONDENSATION AT A FREE ^{4}HE SURFACE

It has been suggested[9] that the condensate fraction in the low density region near a ^{4}He surface is significantly larger than the value in bulk helium of 0.1[7]. Variational Monte Carlo (VMC) simulations by Lewart and Pandharipande[8] of small ($N = 70$) ^{4}He droplets using a Jastrow one-body (JOB) trial wave function give evidence for a condensate fraction which approaches unity as the density goes to zero in the helium surface. However, subsequent calculations by Galli and Reatto[10] have shown that the condensate fraction throughout a helium surface computed using VMC is highly sensitive to the choice of trial wave function. They found that calculations performed using a shadow wave function with a glue term (G-SWF) have enhanced density-density correlations at long wavelengths[11], and a maximum condensate fraction of only 0.5. Significant ripplon excitations are expected to reduce the condensate fraction at the surface, as fewer atoms are able to occupy the zero-momentum state. Quantum evaporation experiments[6] can be interpreted as providing evidence of an enhanced condensate fraction.

To avoid the problem of trial function bias and to include finite-temperature effects, we have used Path Integral Monte Carlo (PIMC) to calculate the density-density correlation functions and condensate fraction at the surface of liquid ^{4}He. We have also used imaginary-time correlation functions to calculate the dispersion relation of surface excitations in a free helium surface, and find good agreement with experimental thin film measurements.

II. PIMC SIMULATION

Our simulation system consisted of ^{4}He atoms, interacting pair-wise with a very accurate potential[12]. Periodic boundary conditions were used with a box size and initial conditions chosen to favor a double-sided film oriented perpendicular to the z-axis. To maintain a stable film and minimize finite size effects, we added an external potential determined from the long-ranged part of the interaction potential and the missing atoms from the other side of the slab, so that atoms on each of the two surfaces saw a potential as if they were at the surface of a semi-infinite slab[13].
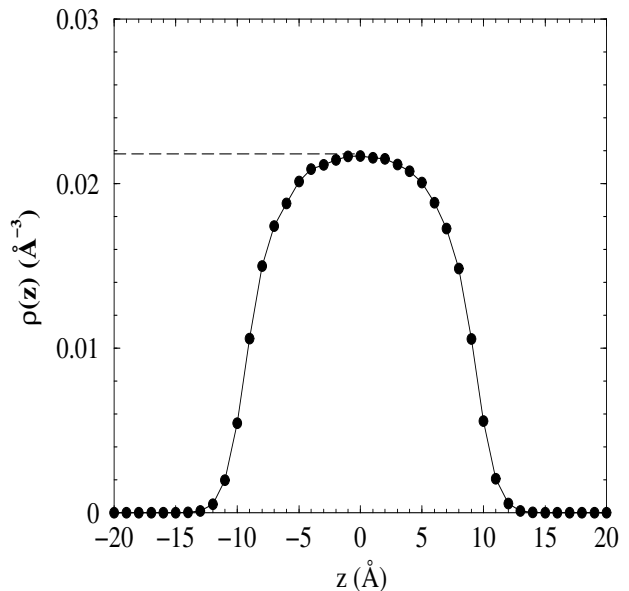

FIG. 1: PIMC density distribution, for an $N = 432$, $T = 0.77$ K semi-infinite ^{4}He slab. The $N = 216$ results are indistinguishable. The dashed line shows the effective helium density felt by atoms at $z > 0$.

Most of the calculations were performed with $T = 0.77$ K, with an imaginary time step of $\tau = 1/20\,\text{K}^{-1}$. We performed simulations of helium slabs containing $N =$

216 and $N = 432$ atoms, with dimensions $24 \times 24 \times 17$ Å and $34 \times 34 \times 17$ Å, respectively. Lower temperature calculations were also done to determine the temperature dependence.

III. THE STATIC STRUCTURE FACTOR

In order to determine the extent to which ripplons are present in a free helium surface, we estimated density-density correlations at the surface[11] with the static structure factor defined as:

$$S(k_{||}; z, z') = \langle \rho_{k_{||}}(z)\rho_{k_{||}}(z') \rangle \qquad (3.1)$$

where $\rho_k(z) \equiv \frac{1}{\sqrt{N(z)}} \sum_i e^{i\mathbf{k} \cdot \mathbf{r}_i} \delta(z_i - z)$, $N(z)$ is the num-
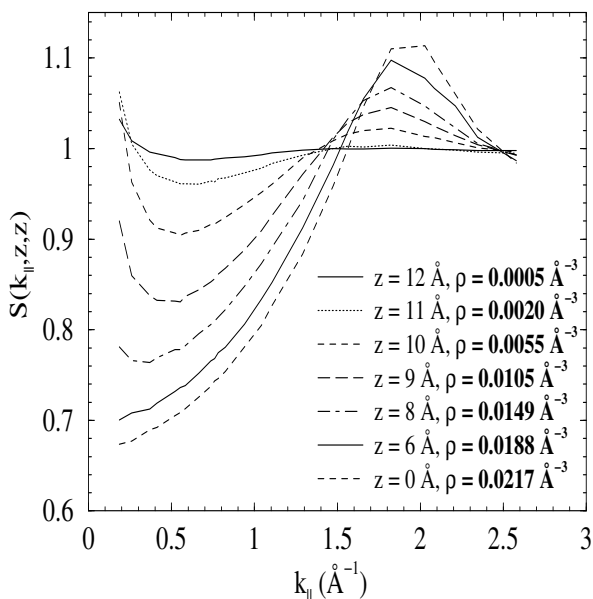

FIG. 2: $S(k_{||}, z, z)$ vs. $k_{||}$ throughout the surface region in an $N = 432$ ^{4}He slab, calculated with PIMC, for $T = 0.77$ K.

ber of particles in the bin at position z and $k_{||}$ is the wave vector parallel to the surface. This measures the correlation between density fluctuations at vertical positions z and z'.

Fig. 2 shows $S(k_{||}, z, z)$ curves as a function of density (z). Each curve is the average of both sides of the slab of eight identical simulations (a total of 7×10^5 Monte Carlo passes). At densities of $\rho(z) = 0.015$ Å^{-3} and below there is a small enhancement of long-wavelength density-density correlations at $k_{||} = 2\pi/L = 0.18$ Å^{-1}, which is evidence for ripplons. However, the curves are closer to the VMC calculations of Galli and Reatto which used a JOB trial wave function than those which used the G-SWF form. This does not imply that the JOB trial wave function is well-suited to representing an inhomogeneous helium system such as a helium slab, but rather the degree to which the G-SWF significantly overestimates the effect of ripplons in a free helium surface. Calculations at $N = 216$ and $T = 0.77$ K agree with the results of Fig. 2 within statistical error, indicating that finite-size effects are negligible. At $T = 0.38$ K, we find a measurable decrease in the long-wavelength correlations. Further studies are needed to establish the temperature dependence.

IV. THE EXCITATION SPECTRUM

The excitation spectrum can be estimated with path integrals using imaginary-time correlation functions[14]. The dynamic structure factor is related to the imaginary-time density-density correlation function by:

$$F(\mathbf{k}, t) = \int_{-\infty}^{\infty} d\omega \, e^{-t\omega} \, S(\mathbf{k}, \omega) \qquad (4.1)$$

$$= \frac{1}{N} \langle \rho_{\mathbf{k}}(t)\rho_{\mathbf{k}}(0) \rangle . \qquad (4.2)$$

To select out the excitations at the free surface, we want to calculate the imaginary-time correlation function of propagating surface modes. W. F. Saam[15] proposed that the lowest quantized hydrodynamic mode (capillary wave) at a free helium surface will have the form

$$\phi_{k0}(\mathbf{r}, t) = \phi_{k0}(z) \, e^{i\mathbf{k} \cdot \mathbf{r}_{||}} \, e^{-i\omega_{k0}t} \qquad (4.3)$$

where

$$\phi_{k0}(z) \propto e^{-\kappa(k)z} \qquad (4.4)$$

and the decay constant $\kappa(k)$ is defined as

$$\kappa(k) = -b_k + (k^2 + b_k^2)^{1/2} \qquad (4.5)$$

$$b_k \equiv \frac{\sigma_0 k^2}{2\rho_0 s^2} \qquad (4.6)$$

where σ_0 is the zero-temperature surface tension, ρ_0 is the bulk density, and s is the zero-temperature sound velocity. To calculate the dispersion relations for excitations of this form, we use $\tilde{\rho}_{\mathbf{k}}$ in Eq. (4.2), defined as

$$\tilde{\rho}_{\mathbf{k}} = \sum_i e^{i\mathbf{k}_{||} \cdot \mathbf{r}_{i||}} \, \phi_k(z_i) \qquad (4.7)$$

where

$$\phi_k(z) = e^{-\kappa(k)(z - z_c)} \qquad (4.8)$$

and $\kappa(k)$ is defined by Eq. (4.5). We defined z_c as the point in the surface at which the average density was equal to 10% of the bulk density.

Extracting the dynamic structure factor by inverting Eq. (4.1) is ill-conditioned in the presence of statistical noise. It has been shown[16] that a maximum entropy method greatly increases the numerical stability. In the maximum entropy method, $S(k, \omega)$ is calculated by minimizing the function

$$\mathcal{F}(S, \alpha) = \frac{e^{-(1/2)Q(S)}}{Z_Q} \times \frac{e^{\alpha \zeta(S)}}{Z_\zeta} \qquad (4.9)$$

where $Q(S)$ is the "likelihood" of the PIMC data given an S and $\zeta(S)$ is the entropy of a given $S(k,\omega)$ defined with respect to some default model, with α an adjustable parameter (also optimized).
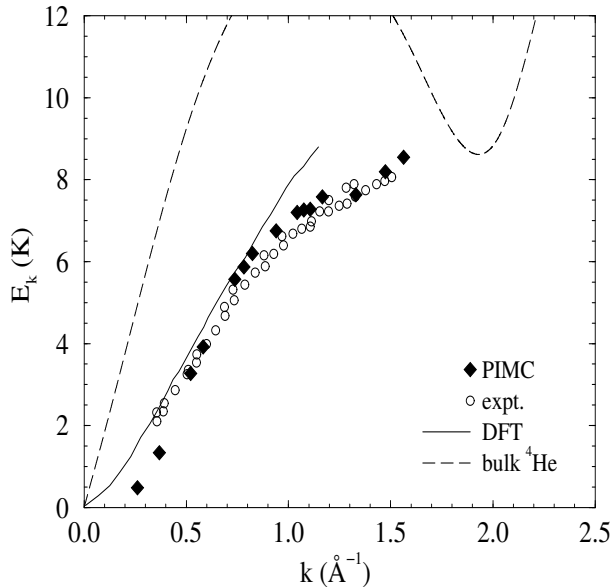

FIG. 3: Dispersion relation of free surface excitations. The results calculated from PIMC and maximum-entropy inversion (filled diamonds) for an $N = 216$, $T = 0.77$ K ^{4}He slab are compared with the experimental thin film data (open circles) of Lauter *et al.* and the DFT results (solid line) of Lastri *et al.* Also shown is the dispersion relation of bulk ^{4}He at SVP (dashed line).

The dispersion energy for a given value of k can be determined from the position of the maximum value of $S(k,\omega)$. Boninsegni and Ceperley[17] found that the position of the main $S(k,\omega)$ peaks for liquid helium agree quite well with experiment, despite significant broadening of the excitation spectrum caused by the maximum entropy procedure. The dispersion energy of the surface excitations as estimated using this procedure are shown in Fig. 3. The two lowest data points, at $k < 0.5$ Å, had significant fitting error and are only qualitatively reliable. Otherwise, we see excellent agreement with the experimental thin film data of [3], including the curvature of the ripplon branch toward the roton minimum, proposed as evidence for roton-ripplon hybridization[18, 19].

V. THE BOSE-EINSTEIN CONDENSATE FRACTION

We define the condensate fraction in the slab geometry by the fraction of atoms at a given value of z having precisely $k_{||} = 0$. (Because $[k_{||}, z] = 0$, we can measure the momentum parallel to the surface simultaneously with the z-position.) The momentum distribution at a dis-

tance z_0 from the center of the slab is given by

$$n_{\mathbf{k}_{||}}(z_0) = \frac{1}{(2\pi)^2} \int d\mathbf{r}_{||} \; e^{-i\mathbf{k}_{||}\cdot\mathbf{r}_{||}} \; n(\mathbf{r}_{||}; z_0) \qquad (5.1)$$

where the off-diagonal single particle density matrix is:

$$n(\mathbf{r}; z) = \frac{1}{\rho(z)Z} \int d\mathbf{r}_1 \cdots d\mathbf{r}_N \; \rho(\mathbf{r}_1, \mathbf{r}_2, \cdots \mathbf{r}_N, \mathbf{r}_1+\mathbf{r}, \mathbf{r}_2, \cdots \mathbf{r}_N; \beta).$$
$$(5.2)$$

and ρ is the many-body density matrix, $Z = \mathrm{Tr}(\rho)$ is the partition function, and $r_{||} \equiv |\mathbf{r}_{||} - \mathbf{r}'_{||}|$. This function can be calculated from PIMC[20] by performing simulations with a single open path. We fix the endpoints of the open path at $z = z_0$, and calculate the distribution of end-to-end distance $n(r_{||}; z_0)$. The condensate fraction at a given point in the surface is:

$$n_0(z_0) = \frac{n(r_{||} \to \infty; z_0)}{n(r_{||} \to 0; z_0)}. \qquad (5.3)$$

Using PIMC, we calculated $n(r_{||}, z)$ throughout the slab. Nonlinear least-squares fitting was used in the region of $r_{||} < 1.5$ Å to get an estimate of $n(r_{||} = 0, z)$, and $n(r_{||} \to \infty, z)$ was calculated by averaging over the region at large $r_{||}$ where $n(r_{||}, z)$ is flat. At the lowest densities, it is not clear whether the $n(r)$'s have reached their asymptotic limit within the finite simulation box. Thus, for those densities, (for $N = 216$ below $\rho(z) = 0.001$ Å^{-3}) our results are upper bounds to the condensate fraction.

The condensate fraction $n_0(z)$ is plotted as a function of average density $\rho(z)$ in Fig. 5, for both $N = 216$ and $N = 432$ helium slabs. As one moves through the surface, the condensate fraction initially increases with decreasing density, due to the decreased zero-point motion from helium-helium interactions, reaching a maximum value of 0.93(3) at $\rho(z) = 0.002$ Å^{-3}. As the average density decreases below this point, the condensate fraction begins to decrease, further evidence for correlated density fluctuations due to ripplons at the surface. This is in qualitative agreement with the G-SWF VMC calculations of Galli and Reatto. However, the G-SWF trial wave function significantly overestimates the degree to which ripplons are present in the surface.

Our results support the model of a free helium surface with ripplons, in which the condensate fraction reaches a maximum at an intermediate density in the liquid-vacuum interface, before decreasing at lower densities. Experimental probes of the surface will indeed see an enhanced condensate fraction as proposed by Griffin and Stringari[9].

VI. LOCAL SUPERFLUIDITY DENSITY ESTIMATOR

In this section, a microscopic Path Integral Monte Carlo (PIMC) estimator of the local contribution to the
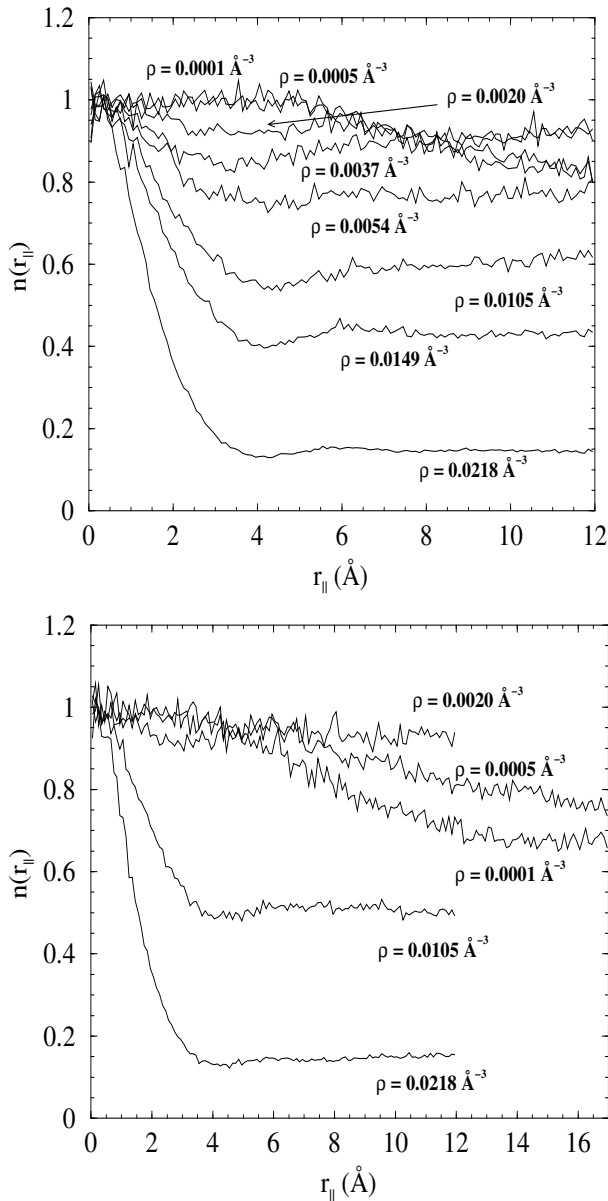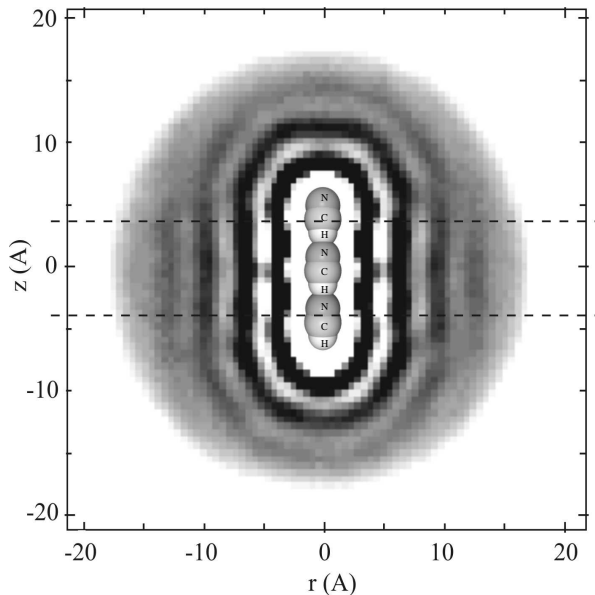
FIG. 6: Average number density of an $N = 500$ ^{4}He-(HCN)$_3$ droplet at $T = 0.38$ K. The grey scale saturates at $\rho = 0.03$ Å^{-3} (black). The dashed lines define the cylindrically-symmetric region used for averaging superfluid density.

noise of the superfluid density. Numerically we find that the same cycle contribution accounts for roughly 80% of the total superfluid density in the systems presented in this paper.

The local superfluid density estimator used by Kwon and Whaley[23] defined the effective normal fluid induced by the anisotropic molecule-helium interaction potential in terms of the average number density distribution of paths in exchange cycles of fewer than six atoms. Although qualitatively interesting, this estimator is not the superfluid response to an imposed rotation, as there is no direct relation between the number of atoms in a permutation cycle and its area.

VII. SUPERFLUIDITY OF HELIUM DROPLETS WITH MOLECULAR IMPURITIES

Molecules confined in helium nanodroplets have been shown to exhibit excitation spectra with clearly resolved rotational fine structure consistent with that of a free rotor, though with an increased moment of inertia. Grebenev et al.[21] have shown that only a few layers of ^{4}He coating the molecule are required to decouple the impurity from the droplet and achieve free rotation. Callegari et al.[22] have suggested that the increased moment of inertia is due to the hydrodynamic response of the impurity rotating through the anisotropic helium density immediately surrounding the molecule. Kwon and Whaley[23] have proposed a model in which a microscopic normal fluid is induced in the first solvation layer by the anisotropy of the molecule-helium interaction.

In order to test our estimator, PIMC simulations were performed on $N = 128$ and $N = 500$ ^{4}He droplets doped with (HCN)$_3$ isomers. Nauta and Miller[32] found that HCN molecules in helium droplets self-assemble into linear chains spaced roughly 4.4 Å apart. The HCN molecules in our simulations were fixed along the z-axis with this spacing. An imaginary time-step of $1/20$ K^{-1} was used. With cylindrical symmetry and precise experimental data over a range of isomer lengths, this system is well-suited for studying superfluidity at a molecular interface.

The number density of a doped helium droplet at $T = 0.38$ K is shown in Fig. 6. The two-dimensional areal density of the first solvation layer was 0.12 Å^{-2}, which is still in the liquid phase for thin ^{4}He films at these temperatures [25]. Even if the density were large enough to be solid in a 2D film, the curved geometry of the film around the HCN molecule could frustrate crystalline order, keeping the first solvation layer in a dense liquid state.
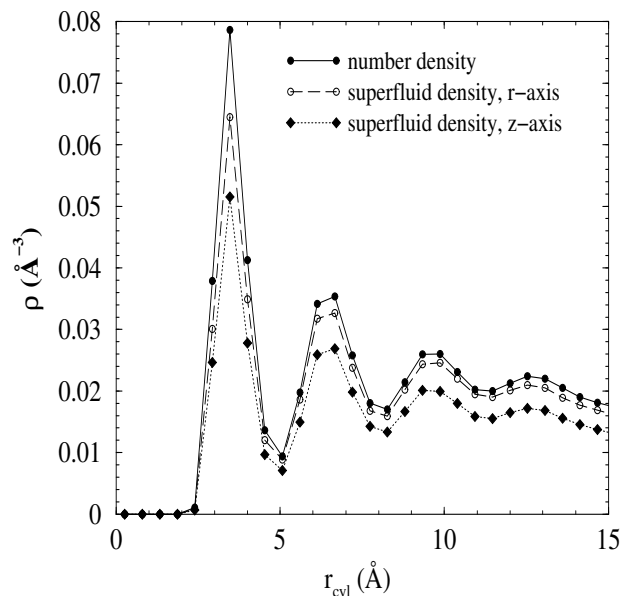

FIG. 7: Superfluid and number density distributions, averaged over the cylindrically-symmetric region of an $N = 500$ ^{4}He-(HCN)$_3$ droplet at $T = 0.38$ K.

We define the change in the moment of inertia due to the helium as the contribution due to the normal fraction in the first layer rotating rigidly with the impurity:

$$\Delta I = \int_{v(\xi)} d\mathbf{r} \, m_4 \, r_\perp^2 \, (\rho(\mathbf{r}) - \rho_s(\mathbf{r})) \qquad (7.1)$$

where $v(\xi)$ is the volume of helium a distance ξ away from the surface of the molecule, $r_\perp$ is the radial distance from the axis of rotation in cylindrical coordinates. Both the estimated statistical error and the uncertainty due to the cut-off were on the order of 10%. The moment of inertia due to the effective normal fluid in the first solvation layer calculated using our PIMC local superfluid

density estimator is in reasonable agreement with the experimental value of $\Delta I = 1240$ amu Å^2 [31], within error bars. We also find that ΔI is effectively independent of temperature below

$T = 1.0$ K. This is because the dominant contribution to the moment of inertia comes from the induced normal fluid at the ends of the isomer, which is almost completely due to anisotropy in the molecular potential.
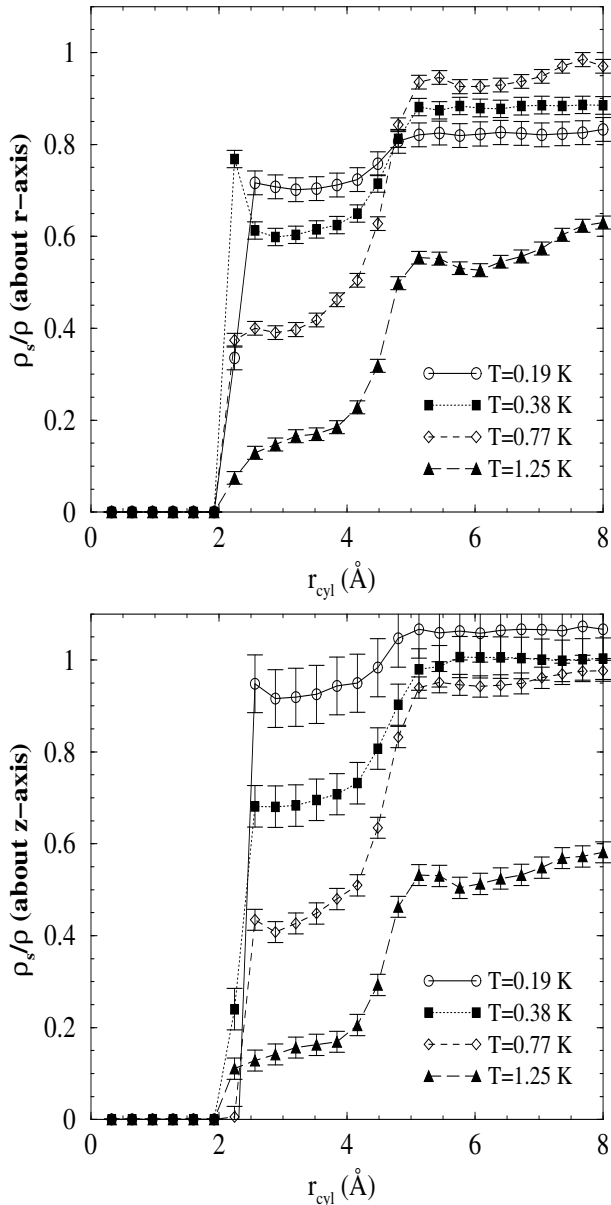

FIG. 8: Superfluid density fraction distributions, averaged over the cylindrically-symmetric region of an $N = 128$ ^{4}He-(HCN)$_3$ droplet at $T = 0.19$, 0.38, 0.77, and 1.25 K. The top graph shows superfluid response about the radial axis, the bottom graph shows superfluid response about the molecule axis.

To quantify the reduced superfluid response in the first layer, we averaged over the cylindrically-symmetric re-

gion of the ^{4}He-(HCN)$_3$ droplet, defined as the region between $z = -3.5$ Å and $z = 3.5$ Å (see Fig. 6). The results of this averaging are shown in Fig. 7. Taking the ratio of the superfluid density to the number density clearly shows a reduced superfluid response in the first layer for rotation about both the radial axis and the molecular axis. At zero temperature, there can be no "normal" density for rotation about the molecular axis because of the cylindrical symmetry, so this reduction must be due to thermal excitations.

Shown in Fig. 8 is the temperature dependence of the superfluid density in the first solvation layer. determined for $N = 128$ ^{4}He-(HCN)$_3$ droplets at $T = 0.19$, 0.38, 0.77, and 1.25 K. At first glance, this result appears to contradict known properties of liquid helium; the superfluid density of bulk helium at 0.75 K is 1.000(1). Theoretical studies of pure $N = 128$ helium clusters show a superfluid transition roughly in agreement with the bulk lambda transition[26]. Pure droplets like those produced for use in scattering experiments, with several thousand atoms at $T = 0.38$ K, should have a superfluid fraction very close to unity. However, the helium in the first layer coating the impurity molecule more closely resembles a two-dimensional system than a three-dimensional system, because the motion of the helium atoms is restricted by the He-HCN potential to be primarily on the cylindrical surface circumscribing the (HCN)$_3$ impurity. Two-dimensional helium films have been shown to have a Kosterlitz-Thouless type of superfluid transition at temperatures significantly lower than T_λ [27, 28]. The reduction in the transition temperature is due to the reduced dimensionality, increasing the phase space for long wavelength fluctuations, and the lowering of the "roton" gap. A similar temperature-dependent reduction in the superfluid response of the first layer of helium surrounding the ends of the isomer was not observed.

To extract the average superfluid density fraction in the first layer from the distributions plotted in Fig. 8, we integrate over the superfluid density and number density in the first layer and take the ratio:

$$\frac{\rho_s}{\rho} = \frac{\int_0^{r_1} dr_{cyl}\,\rho_s(r_{cyl})}{\int_0^{r_1} dr_{cyl}\,\rho(r_{cyl})}, \qquad (7.2)$$

where r_1 is the position of the density minimum between the first and second solvation layers. The average superfluid density in the first solvation layer as a function of temperature is shown in Fig. 10. The transition is very broad due to the small number of atoms (~ 30) in the first layer. It shows the onset of superfluidity at roughly 1 K. The superfluid density about the molecule axis (z-axis) goes to unity as the temperature goes to zero, as the density is symmetric about this axis. The normal fluid response from rotating about the radial axis (r-axis) combines both thermal effects and effective normal fluid induced by rotating through the anisotropic

helium density, and because of this, does not go to zero at $T = 0$ K[22].

We have determined that only a small fraction of the particles in the first layer are localized (not permuting) at T=0.38 K and below, as shown in Fig. 9. Though many of the permutations are between atoms within the same layer, the first layer is not cut off from the rest of the fluid. Below 1 K, the majority of the atoms in the droplet are part of exchange cycles with atoms in both the first layer and the rest of the droplet. However, in terms of excitations, the first layer is well represented as a 2D superfluid.
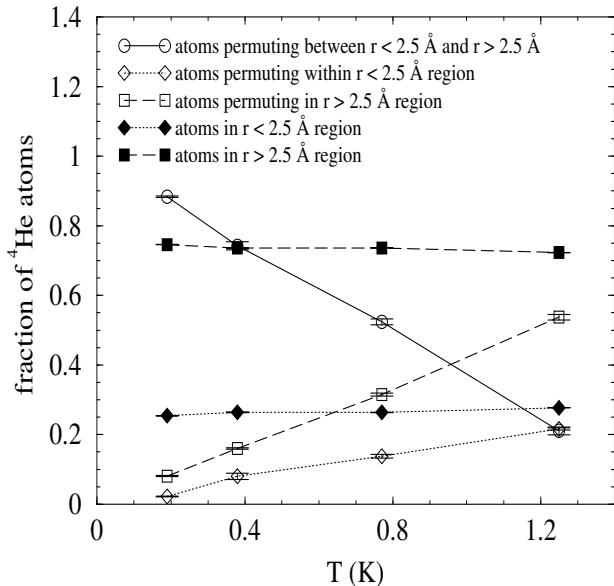

FIG. 9: Exchange behavior of the first layer (defined as 2.5 Å or less from the surface of the $(HCN)_3$ isomer) as a function of temperature. A permutation cycle was considered to be part of the first layer if more than $M/2$ consecutive time slices were contained within it, where M is the number of imaginary time slices per atom.

To compare the effects of density on the thermally-induced normal fluid in the first layer, we calculated the superfluid density distribution for $N = 128$ ^{4}He-$(HCN)_3$ droplets at T=0.19, 0.38, 0.77, and 1.25 K, with a ^{4}He-HCN interaction reduced by a factor of two in order to reduce the density in the first solvation layer. The density in the first layer decreased by $\sim 15\%$, corresponding to an average coverage of 0.10 Å^{-2}. The difference in coverage caused a 20% reduction in the superfluid response about the radial axis at T=0.19 K and T=0.38 K. At higher temperatures, the superfluid response was unchanged within the estimated error bars. The superfluid response about the molecule axis (z-axis) was unchanged within error bars. This is further evidence that the normal response in the first layer is due to both the anisotropy of the molecular potential and thermal excitations.

Using PIMC and a local superfluid density estimator, we find that the first solvation layer surrounding an $(HCN)_3$ isomer has significant thermal excitations at temperatures as low as T=0.19 K, with a superfluid transition temperature similar to that of a two-dimensional system. It remains to be seen how strongly these thermal excitations are present in droplets with different dopants; this is the first observation of thermal excitations in a helium droplet at such low temperatures. Although we find this effect only makes a small contribution to the moment of inertia of this system, it may explain the anomalous Q branch observed in helium droplets doped with long linear impurities. The role of thermal excitations could also be tested by varying the temperature of the droplet, by adding ^{3}He atoms.
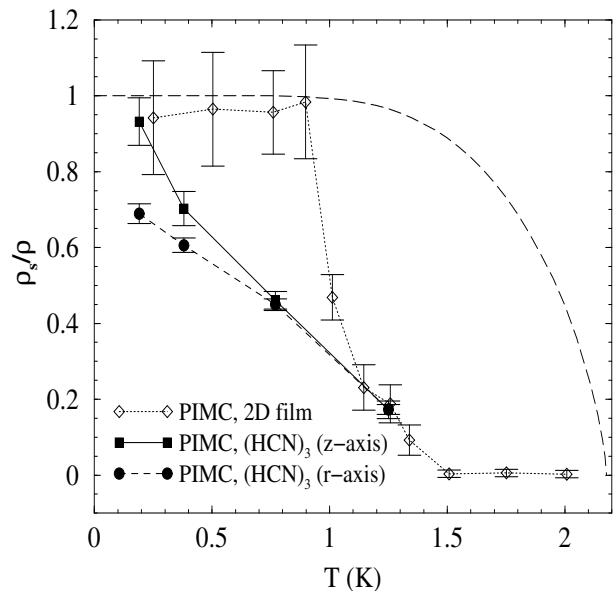

FIG. 10: Superfluid density fraction of the cylindrically-symmetric portion of the first layer of an $N = 128$ ^{4}He-$(HCN)_3$ droplet vs. temperature, calculated using Eq. (7.2). The first layer in these systems has an estimated coverage of $\sigma = 0.12$ Å^{-2}. Superfluid response about both the molecule axis (solid squares) and radial axis (solid circles) are presented. Also shown are the PIMC results of Gordillo et al (open diamonds), for a 2D ^{4}He film with $\sigma = 0.051$ Å^{-2}. For reference, the superfluid transition in bulk ^{4}He is included (dashed line).

[1] E. W. Draeger and D. M. Ceperley, Phys. Rev. Letts. **89**, 015301 (2002).

[2] E. W. Draeger and D. M. Ceperley, Phys. Rev. Lett. **90**, 065301 (2003).

[3] H. J. Lauter, H. Godfrin, V. L. P. Frank, and P. Leiderer, Phys. Rev. Lett. **68**, 2484 (1992).

[4] D. O. Edwards and W. F. Saam, in *Progress in Low Temperature Physics VII A*, edited by D. F. Brewer (North-Holland, Amsterdam), p. 283, 1978.

[5] A. Lastri, F. Dalfovo, L. Pitaevskii, and S. Stringari, J. Low Temp. Phys. **98**, 227 (1995).

[6] A. F. G. Wyatt, Nature **391**, 56 (1998).

[7] O. Penrose and L. Onsager, Phys. Rev. **104**, 576 (1956).

[8] D. S. Lewart, V. R. Pandharipande, and S. C. Pieper, Phys. Rev. B **37**, 4950 (1988).

[9] A. Griffin and S. Stringari, Phys. Rev. Letts. **76**, 259 (1996).

[10] D. E. Galli and L. Reatto, J. Low Temp. Phys. **113**, 223 (1998).

[11] D. E. Galli and L. Reatto, J. Phys. Condens. Matter **12**, 6009 (2000).

[12] R. A. Aziz, A. R. Janzen, M. R. Moldover, Phys. Rev. Letts. **74**, 1586 (1995).

[13] M. Wagner and D. M. Ceperley, J. Low Temp. Phys. **94**, 161 (1994).

[14] D. M. Ceperley, Rev. Mod. Phys. **67**, 279 (1995).

[15] W. F. Saam, Phys. Rev. B **12**, 163 (1975).

[16] J. E. Gubernatis, M. Jarrell, R. N. Silver, and D. S. Sivia, Phys. Rev. B **44**, 6011 (1991).

[17] M. Boninsegni and D. M. Ceperley, J. Low Temp. Phys. **104**, 339 (1996).

[18] E. Krotscheck, S. Stringari, and J. Treiner, Phys. Rev. B **35**, 4754 (1987).

[19] L. Pitaevskii and S. Stringari, Phys. Rev. B **45**, 13133 (1992).

[20] D. M. Ceperley and E. L. Pollack, Can. J. Phys. **65**, 1416 (1987).

[21] Grebenev, S., J. P. Toennies and A. F. Vilesov, Science **279**, 2083 (1998).

[22] Callegari, C., A. Conjusteau, I. Reinhard, K. K. Lehmann, G. Scoles and F. Dalfovo, Phys. Rev. Lett. **83**, 5058 (1999).

[23] Kwon, Y. and K. B. Whaley, Phys. Rev. Lett. **83**, 4108 (1999).

[24] Pollack, E. L. and D. M. Ceperley, Phys. Rev. B **36**, 8343 (1987).

[25] Bishop, D. J., J. E. Berthold, J. M. Parpia and J. D. Reppy, Phys. Rev. B **24**, 5047 (1981).

[26] Sindzingre, P., M. L. Klein and D. M. Ceperley, Phys. Rev. Lett. **63**, 1601 (1989).

[27] Ceperley, D. M., and Pollock, E. L., Phys. Rev. B **39**, 2084 (1989)

[28] Nyéki, J., R. Ray, V. Maidanov, M. Siqueira, B. Cowan and J. Saunders, J. Low Temp. Phys. **101**, 279 (1995).

[29] Gordillo, M. C. and D. M. Ceperley, Phys. Rev. B **58**, 6447 (1998).

[30] Kim, K. and W. F. Saam, Phys. Rev. B **48**, 13735 (1993).

[31] Nauta, K., private communication (2001).

[32] Nauta, K. and R. E. Miller, Science **283**, 1895 (1999).

[33] Goyal, S., D. L. Schutt and G. Scoles, Phys. Rev. Lett. **69**, 933 (1992).

[34] Pi, M., R. Mayol and M. Barranco, Phys. Rev. Lett. **82**, 3093 (1999).

[35] Lehmann, K. K., Mol. Phys. **97**, 645 (1998).

[36] Toennies, J. P. and A. F. Vilesov, Annu. Rev. Phys. Chem. **49**, 1 (1998).

[37] Atkins, K. M. and J. M. Hutson, J. Chem. Phys. **105**, 440 (1996).

[38] Kwon, Y., P. Huang, M. V. Patel, D. Blume and K. B. Whaley, J. Chem. Phys. **113**, 6469 (2000).